Biogeosciences Discuss., 11, 6119–6149, 2014
www.biogeosciences-discuss.net/11/6119/2014/
doi:10.5194/bgd-11-6119-2014

Biogeosciences Discussions
Open Access

Disparities between *Phaeocystis* in situ and optically-derived carbon biomass and growth rates: potential effect on remote-sensing primary production estimates

L. Peperzak[1,2], H. J. van der Woerd[1], and K. R. Timmermans[2]

[1]Institute for Environmental Studies (IVM), VU University Amsterdam, the Netherlands
[2]Royal Netherlands Institute for Sea Research/NIOZ, Department of Biological Oceanography, Texel, the Netherlands

Received: 7 February 2014 – Accepted: 8 April 2014 – Published: 29 April 2014

Correspondence to: L. Peperzak (louis.peperzak@nioz.nl)

Published by Copernicus Publications on behalf of the European Geosciences Union.

Abstract

The oceans play a pivotal role in the global carbon cycle. Unfortunately, the daily production of organic carbon, the product of phytoplankton standing stock and growth rate cannot be measured globally by discrete oceanographic methods. Instead, optical proxies from Earth-orbiting satellites must be used. To test the accuracy of optically-derived proxies of phytoplankton physiology and growth rate, standard ex situ data from the wax and wane of a *Phaeocystis* bloom in laboratory mesocosms were compared with hyperspectral reflectance data. Chlorophyll biomass could be estimated accurately from reflectance using specific chlorophyll absorption algorithms. However, the conversion of chlorophyll (Chl) to carbon (C) was obscured by the observed increase in C : Chl under nutrient-limited growth. C : Chl was inversely correlated ($r^2 = 0.88$) with Photosystem II quantum efficiency (Fv/Fm), the in situ fluorometric oceanographic proxy for growth rate. In addition, the optical proxy for growth rate, the quantum efficiency of fluorescence φ was linearly correlated to Fv/Fm ($r^2 = 0.84$), but not – as by definition – by using total phytoplankton absorption, because during nutrient-limited growth the concentrations of non-fluorescent light-absorbing pigments increased. As a consequence, none of the three proxies (C : Chl, Fv/Fm, φ) was correlated to carbon or cellular phytoplankton growth rates. Therefore, it is concluded that although satellite derived estimates of chlorophyll biomass may be accurate, physiologically-induced nonlinear shifts in growth rate proxies may obscure accurate phytoplankton growth rates and hence global carbon production estimates.

1 Introduction

Approximately half of the global photosynthetic CO_2 to organic carbon conversion takes place in marine waters (Field et al., 1998). Unfortunately, global daily CO_2 fixation, the product of phytoplankton standing stock and growth rates cannot be measured directly for the world oceans. Phytoplankton biomass and growth rates can be assessed di-

BGD
11, 6119–6149, 2014

rectly and accurately by standard oceanographic techniques, but these miss the spatial coverage of the optical instruments on board Earth-orbiting satellites. On the other hand, optically-derived estimates of phytoplankton biomass and growth rates are less accurate than ship-board data (Abbott and Letelier, 1999; Carder et al., 2003; Behrenfeld et al., 2005; Huot et al., 2005; Astoreca et al., 2009; Martinez-Vicente et al., 2013). Here we report, to our knowledge for the first time ever, on the simultaneous evaluation of standard oceanographic and state-of-the-art optical techniques for gauging both phytoplankton biomass and carbon growth rates, hence CO_2 fixation.

Optical estimates of the oceanic carbon concentration for growth rate estimations can be made from the particulate backscatter coefficient bbp (Behrenfeld et al., 2005), but this coefficient is non-specific for phytoplankton or valid only for low chlorophyll *a* concentrations (Martinez-Vicente et al., 2013). Alternatively, the phytoplankton-specific chlorophyll concentration can be estimated from water-leaving radiance as absorbance (Carder et al., 2003). However, a robust carbon to chlorophyll ratio (C : Chl) is then needed to convert chlorophyll into carbon (Sathyendranath et al., 2009). Unfortunately, this ratio is not constant.

A second optical growth rate proxy is the phytoplankton-specific red chlorophyll fluorescence relative to absorbance (φ). By definition this "quantum efficiency of fluorescence" is the ratio of the number of fluoresced photons to the number of photons absorbed by the phytoplankton, i.e. by all cellular photo-pigments (Abbott and Letelier, 1999; Huot et al., 2005). If under nutrient limitation the production of chlorophyll stops and fluorescence increases, both C : Chl and φ will increase (Kiefer, 1973; Falkowski et al., 1992; Behrenfeld et al., 2009).

In "standard" oceanographic measurements, carbon fixation, chlorophyll and other photopigment concentrations are analysed in discrete water samples (ex situ), as is the quantum efficiency of Photosystem II (Fv/Fm), the equivalent of φ (Kromkamp and Foster, 2003). In other words, many potentially suitable proxies for primary production estimates from space are available, but their concrete applicability is uncertain.

BGD
11, 6119–6149, 2014

Besides the lack of specificity, an inherent problem in the optical approach of organic carbon production is that estimates of carbon and chlorophyll are used in both biomass and growth rate proxies. Moreover, doubt has been raised if the variability in remote-sensed phytoplankton physiology (φ) is due to physiological changes in the phytoplankton, or due to environmentally driven biases in algorithms needed to estimate φ (Huot et al., 2005).

In order to study the variability in phytoplankton biomass, growth rate, absorbance and fluorescence under variable, but fully-controlled conditions, mesocosm experiments were conducted where detailed "standard" oceanographic measurements were combined with close-sensing hyperspectral measurements. Phytoplankton dynamics in the mesocosms were experimentally manipulated under semi-natural conditions of temperature, irradiance and turbulence (Peperzak et al., 2011). The prymnesiophyte *Phaeocystis* globosa, a key species in marine primary production was used as test organism (Wassmann et al., 1990; Smith et al., 1991; DiTullio et al., 2000; Vogt et al., 2012). The ultimate aim of the experiments was to test the null-hypothesis that there is no difference between a range of standard oceanographic and optical techniques for measuring phytoplankton biomass and growth rate.

2 Methods

2.1 Experimental

The flagellate life-form of *Phaeocystis* globosa strain Pg6-I ("*Phaeocystis*") was inoculated in two duplicate 140 L mesocosms filled with 0.2 µm filtered nutrient-poor Atlantic Ocean water that had been diluted with Milli-Q^{TM} to a salinity of 34 g kg^{-1}. A detailed description of the mesocosms is given in (Peperzak et al., 2011). Temperature during *Phaeocystis* growth was kept at 15 °C. Irradiance was provided in a semi-sinusoidal light dark (16 : 8 h) cycle with a maximum surface PAR of 41 W m^{-2} in mesocosm 1 and 45 W m^{-2} in mesocosm 2. Turbulence of the water was provided by pumping surface

BGD
11, 6119–6149, 2014

water to the bottom of the mesocosm at a turn-over rate of 1 h^{-1}. The water was enriched with macronutrients to: 30 µM NO_3^-, 6.3 µM PO_4^{3-}, and trace metals and vitamin B1 (Peperzak et al., 2011). On day 8 of the experiment, when cells were in stationary growth phase, mesocosm 1 received enrichment with the initial nutrient concentrations to examine the effect of alleviation of nitrogen limitation on the physiological and optical properties of *Phaeocystis*.

2.2 Sampling

Water samples were taken in the middle of the light period (13:00 h, Local Time) to measure salinity, pH, cell abundance, dissolved inorganic nitrogen (DIN), soluble reactive phosphorus (SRP), HPLC pigments including chlorophyll *a* (Chl *a*), chlorophyll *c*2 and *c*3 (summed as Chl *c*) and carotenoids, particulate organic carbon (POC) and nitrogen (PON) and PAM (Walz, Water PAM^{TM}) derived Photosystem II quantum efficiency (Fv/Fm). A detailed description of the analyses is provided elsewhere (Peperzak et al., 2011). See Table 1 for a list of measured and derived variables.

Surface irradiance (W m^{-2} nm^{-1}), used to convert radiance (W m^{-2} nm^{-1} sr^{-1}) to reflectance (R, sr^{-1}), was measured prior to and after the experiment. In addition, phytoplankton absorption was measured daily at 13:00 h using a 0.55 L integrating cavity absorption meter or ICAM (a-sphere^{TM}, HobiLabs, Tucson, AZ, USA). ICAM-absorption data (a_{ph}, m^{-1}) were blank-corrected daily by subtracting the absorption of filtered seawater, then divided by chlorophyll *a* or *c* concentrations to obtain the chlorophyll-specific absorption coefficients (a^*_{Chl}, m^2 (mg chlorophyll)$^{-1}$) in both the exponential and the stationary *Phaeocystis* growth phase. *Phaeocystis* spectra of a^*_{Chl}, together with reflectance data, were used to determine the appropriate wavelengths in algorithms for the estimation of chlorophyll *a* (*c*) absorption from reflectance spectra. Details of the ICAM-absorption, irradiance and radiance measurements are provided elsewhere (Peperzak et al., 2011).

BGD
11, 6119–6149, 2014

2.3 Absorption and fluorescence algorithms

Optical proxies were derived from water leaving radiance ($W\,m^{-2}\,nm^{-1}\,sr^{-1}$) spectra that were measured every 15 min with a TriOS RAMSES-ACC-VIS hyperspectral sensor (320–950 nm in 190 channels) at an angle 50° off nadir at 0.08 m above the water surface. Four reflectance spectra from the middle of the light period (13:00–14:00 h) were averaged and algorithms were applied for the estimation of absorption by chlorophyll *a* and *c* ($a_{Chl\,a}$ and $a_{Chl\,c}$) and emission near the 682 nm fluorescence band (F). The chlorophyll *a* (*c*) absorption was calculated from reflectance spectra by a 4-wavelength absorption algorithm (ARP-4$\lambda_{Chl\,c}$) (Appendix A). F was calculated by using a fluorescence line height (FLH) method (Appendix A).

In each of the two mesocosms a TriOS RAMSES-ACC-VIS hyperspectral sensor was mounted at the bottom that registered the irradiance every 15 min. From this signal the wavelength-dependent attenuation in the mesocosm was derived, that was corrected water absorption and scattering and converted to the total number of absorbed photons by *Phaeocystis* cells. The fluorescence line height in the reflection spectrum measured above water was converted to the emission under water, integrated over the full spectrum and in all direction (see Appendix A for more details). The phytoplankton quantum efficiency (φ_{ph}) was calculated by dividing the emitted energy in the fluorescence band by the total absorbed energy ($\mu mol\,photons\,m^{-2}\,s^{-1}$).

2.4 Statistics

To test the null hypothesis that there is no difference between means of variables measured in the two mesocosms, two-sample t tests were performed in SYSTAT™ version 12. Linear regression equations were calculated in SYSTAT™ or Excel™ 2003. Non-linear regression was performed in XLFit™ 4.3. 95 % confidence intervals (±95 % c.i.) around a variable mean m were calculated from a t distribution using n observations (days), $n-1$ degrees of freedom and the standard deviation of the mean sd as: $m \pm 95\,\%$ c.i. $= m \pm t(0.05; n-1) \times sd/\sqrt{n}$. The standard error ($= sd/\sqrt{n}$) provided in linear re-

BGD
11, 6119–6149, 2014

gression by SYSTAT™ was used to calculate 95 % confidence intervals of regression slopes.

3 Results

3.1 Phytoplankton dynamics (ex situ observations)

Inoculation of the mesocosms was followed by a three day exponential increase in *Phaeocystis* cell abundance, Chl *a*, Chl *c*, POC and PON concentrations (Fig. 1a, c–f). Compared to mesocosm 1, the higher surface irradiance in mesocosm 2 led to 17 % more cells on day 5, when the stationary growth phase was reached in both mesocosms due to nitrogen limitation (Fig. 1b). In both mesocosms, cell abundances in stationary growth phase decreased with an average rate of $-0.07\,d^{-1}$. The 30 µM nitrate in the nutrient-spike added to mesocosm 1 on day 8, was already depleted by *Phaeocystis* on day 9 (Fig. 1b) and incorporated as PON (Fig. 1f). In addition, *Phaeocystis* cells, Chl *a* and Chl *c* concentrations increased after the nutrient-spike (Fig. 1a, c and d). In a separate experiment (no data shown), in which a mesocosm 2 water sample on day 10 was spiked with only nitrate, the resumption of cell growth and an increase in Fv/Fm confirmed that nitrogen was the limiting element.

3.2 Physiology and pigment composition (ex situ observations)

After the depletion of DIN on day 4, Fv/Fm declined in both mesocosms (Fig. 2a), while the C : Chl ratios increased (Fig. 2c). The nutrient-spike on day 8 in mesocosm 1 caused a temporary increase in Fv/Fm (Fig. 2a) and led to significantly lower C : N ($t = -25.2$, df = 5, $p < 0.001$) and C : Chl ratios ($t = -8.5$, df = 5, $p < 0.001$) in mesocosm 1 relative to mesocosm 2 (Fig. 2b and c). The difference in Carotenoids: Chl between mesocosm 1 and 2 (Fig. 2d) from day 9 onwards was also significant ($t = -6.8$, df = 5,

BGD
11, 6119–6149, 2014

$p < 0.01$). Thus, the nutrient-spike on day 8 caused a shift in Fv/Fm, C : N, C : Chl and Carotenoids: Chl (Fig. 2a–d).

3.3 Absorption and fluorescence (optical observations)

3.3.1 ICAM absorption

The ICAM absorption spectra of mesocosm water samples contained three major peaks: at 438 nm (Chl *a*), 466 nm (Chl *c*) and 674 nm (Chl *a*). In the exponential growth phase, a^*_{Chl} was lower than in the stationary growth phase, due to the increase in Carotenoids after nitrogen was depleted (Fig. 2d). These differences in a^*_{Chl} between exponential and stationary growth phase were significant at 438 and 466 nm, but not at 674 nm (Table 2).

3.3.2 Reflectance absorption

The specific chlorophyll *a* and *c* absorption (aChl *a* and aChl *c*) computed from reflectance spectra (Fig. 3a and b) closely resembled the development of *Phaeocystis* cell abundance and Chl *a* and *c* concentrations (Fig. 1a, c and d). In both mesocosms, total Chl absorption, $a_{\mathrm{Chl}\ a\ (c)}$ correlated well with HPLC-measured Chl *a* and Chl *c* concentrations (Fig. 3c and d) and the regression slopes of the two variables in the mesocosms were not significantly different (Table 3). When the data of both mesocosms were split by growth phase, the exponential phase (day 1 to 4) regression equations accurately (both $r^2 = 0.98$) estimated both Chl *a* and Chl *c* (Fig. 3e and f). The stationary phase (day 5 to 14) regression intercepts between $a_{\mathrm{Chl}\ a\ (c)}$ and Chl *a* and Chl *c* concentrations were lower than in exponential growth phase (Fig. 3e and f), although not significantly (Table 3). This means that application of the regression equations combining both growth phases (Table 3), will lead to small underestimations of Chl *a* and Chl *c* concentrations in the exponential growth phase, and small overestimations of Chl *a* and Chl *c* concentrations in the stationary phase (Fig. 3e and f).

BGD
11, 6119–6149, 2014

3.3.3 Fluorescence

Fluorescence emission estimated from the water leaving radiance (Fig. 4a) resembled *Phaeocystis* cell dynamics (Fig. 1a) and was well correlated with Chl *a* (Fig. 4b; overall $r^2 = 0.81$, Table 4). When the data of both mesocosms was split by growth phase, the stationary phase (day 5 to 14) regression slope and intercept were significantly different from those in exponential phase (day 1 to 4) (Fig. 4c, Table 4). This means that according to expectation, nutrient-stressed cells in stationary growth phase have higher fluorescence intensity per unit chlorophyll.

3.4 Fluorescence quantum efficiency (optical observations)

The fluorescence efficiency (φ_{ph}) calculated as mol photons emitted as fluorescence divided by the mol photons absorbed by the phytoplankton pigments increased during exponential growth, stabilized from day 5 to 8 and then decreased (Fig. 5). No apparent change in φ_{ph} was observed in response to the nutrient-spike on day 8 to mesocosm 1.

3.5 Carbon growth rate and proxy comparison

In order to relate dynamics in light absorption and fluorescence to *Phaeocystis* physiology in the different growth phases, the dynamics of carbon growth rate (μ_{POC}) was compared to Fv/Fm, C : Chl and φ_{ph} (Fig. 6a–c). Because the cellular Chl *c* content of *Phaeocystis* is about the same as the cellular Chl *a* content (Fig. 1c and d) and total chlorophyll (Chl) was linearly correlated to Chl *a* (Chl = 2.28× Chl *a*, $r^2 = 0.99$), C : Chl was used rather than C : Chl *a* and C : Chl *c* separately.

The proxy comparison showed hyperbolic relations of μ_{POC} with C : Chl and Fv/Fm with highly variable values at $\mu_{POC} \sim 0.0\,d^{-1}$ (Fig. 6a and b). As could be expected from Fig. 6a and b, Fv/Fm was inversely linearly correlated to C : Chl ($r^2 = 0.88$). The good correlation implies that under the present experimental conditions Fv/Fm and

BGD
11, 6119–6149, 2014

C : Chl, as measured either in water samples or derived from water-leaving radiance are directly comparable physiological proxies.

When the fluorescence quantum efficiency is plotted against carbon growth rate (Fig. 6c) two clusters of data can be observed: a low $\varphi_{ph} \approx 1.1$ in exponential phase and a high and fluctuating φ_{ph}($\varphi_{ph} \approx 1.5$) in stationary phase. Because a distinction between exponential and stationary growing phytoplankton populations cannot be made a priori and because φ_{ph} covers a large range in carbon growth rates, it appears that in both mesocosms φ_{ph} is a poor proxy for *Phaeocystis* primary production.

4 Discussion

The aim of the mesocosm experiments was to investigate a relation between optical remote sensing and "standard" oceanographic measurements of phytoplankton physiology during different growth phases (here: nitrogen-controlled growth) of *Phaeocystis* and to infer possible implications for estimates of primary productivity. The standard physiological and reflectance measurements, in combination with the effect of a nutrient-spike to one mesocosm, proved that growth of *Phaeocystis* was indeed nitrogen-limited during the experiments. By measuring the in situ fluorescence (F) increase due to nitrogen limitation, and the phytoplankton pigment absorption (a_{ph}), an optical estimate of the quantum efficiency of fluorescence $\varphi_{ph}(= F/a_{ph})$ could be made. It is shown that of the physiological diagnostics neither φ_{ph}, nor Photosystem II quantum efficiency (Fv/Fm) nor C : Chl are reliable estimators of variability in phytoplankton growth rates. This may have consequences for global carbon fixation estimates using remote sensing data assessing phytoplankton physiology.

4.1 Phytoplankton dynamics

Temperature, salinity, irradiance and pH were at or near values for optimum *Phaeocystis* growth (Peperzak, 2002). Exponential phase growth rate ($\mu = 0.7\,d^{-1}$) and station-

BGD
11, 6119–6149, 2014

ary phase mortality rate ($d = -0.07\,d^{-1}$) were equal to the rates obtained in cultures of *P. globosa* strain Ph91 (Peperzak et al., 2000a, b). The carbon and photopigment contents of *Phaeocystis* in the mesocosms were comparable to published values, although cellular Chl *a* and Chl *c* content were relatively low (Table 5). On the other hand, the fucoxanthin to Chl *a* ratio was high which is probably caused by (1) an adaptation to the low irradiance environment where this flagellate can thrive (Peperzak, 1993; Seoane et al., 2009) and/or (2) the effect of nitrogen-limited growth on the Carotenoids: Chl ratio (Fig. 2d). In mesocosm 2 *Phaeocystis* in stationary phase reached a C : N of 20, which is equal to the subsistence quota of 0.05 mol N mol C^{-1} in diatoms (Edwards et al., 2003). The rapid depletion of nitrate during the initial days of the experiment and the instant decline in C : N, combined with the decrease in C : N, resumption of cell growth and increase in Fv/Fm after the nutrient-spike, convincingly showed that *Phaeocystis* was nitrogen-limited in the stationary phase.

The physiological indicator Fv/Fm declined when nitrogen had been depleted on day 4. In addition, C : Chl increased. Both indicators responded directly following the nutrient-spike to the nitrogen-depleted *Phaeocystis* on day 8. C : Chl was inversely linearly correlated with Fv/Fm, but carbon growth rate was not. This can be explained by the fact that both Fv/Fm and C : Chl declined continuously after nitrogen depletion while cell division immediately halted on day 5. As a consequence, Fv/Fm and C : Chl not only signal physiological change, they are also indicative of the persistence of nitrogen depletion in *Phaeocystis*. A comparable conclusion was reached for the decline of Fv/Fm and the duration of nitrogen depletion in the diatom *Thalassiosira pseudonana* (Parkhill et al., 2001). On the other hand, under balanced growth conditions, i.e. steady-state nitrogen-limited growth, the value of Fv/Fm in *T. pseudonana* was high and comparable to the value in nutrient-replete cultures (Parkhill et al., 2001). In other words, the steady 10 day change after an abrupt nitrogen depletion make that Fv/Fm and C : Chl are not good indicators of real nutrient-limited phytoplankton growth rates.

In the early stationary phase (day 4–8), the 10 % lower surface irradiance in mesocosm 1 led to a slightly lower (94 ± 21) not significantly different C : Chl than in meso-

BGD
11, 6119–6149, 2014

cosm 2 (106±28). Comparable minor effects on cellular chlorophyll contents have been measured in *Phaeocystis* cultured at 10 and 100 µmol photons $m^{-2} s^{-1}$ (Astoreca et al., 2009). Far more important than the (relatively weak) effect of surface irradiance on C : Chl was the factor 10 variability in C : Chl when *Phaeocystis* went from the exponential (C : Chl = 30) to the late stationary growth phase (C : Chl = 200, Fig. 2c and Table 5). This variability confirms that chlorophyll concentration is not a reliable indicator of phytoplankton biomass (Behrenfeld et al., 2009; Kruskopf and Flynn, 2006), which has implications for the correct conversion of chlorophyll to carbon in chlorophyll-based primary production models (Cloern et al., 1995; Sathyendranath et al., 2009).

4.2 Pigments and absorption

Nitrogen depletion led to increases in Carotenoids concentrations relative to chlorophyll. Comparable increases in light absorption under nitrogen limitation, due to increased Carotenoid: Chl *a* ratios, have been observed in other phytoplankton species (Heath et al., 1990; Staehr et al., 2002). The increase of Carotenoids to Chl ratio had a direct effect on the estimation of light absorption from the reflection spectra and ICAM measurements. The excellent correlations (Table 3) between $a_{\text{Chl } a}$ and $a_{\text{Chl } c}$ and respectively Chl *a* and Chl *c* concentrations in exponential phase (both $r^2 = 0.98$) were lower in stationary phase ($0.59 < r^2 < 0.82$). Besides more variability in stationary phase, a_{Chl} was lower than in exponential phase due to interference by Carotenoids in the reflection spectrum. This interference was more pronounced for $a_{\text{Chl } c}$ than for the $a_{\text{Chl } a}$ (Table 3), because the $a_{\text{Chl } c}$ algorithm employs wavelengths from 450 to 480 nm (Appendix A, Eq. A2) where Carotenoids absorption is more pronounced (Fujiki and Taguchi, 2002; Lubac et al., 2008).

The interference of Carotenoids in stationary phase will increase when total pigment absorption (a_{ph}) will be measured instead of specific chlorophyll absorption. It is not surprising, therefore, that by using the ICAM data (400 to 672 nm) the correlation of absorption with Chl was lower ($r^2 = 0.74$) than when using the Chl *a* and Chl *c* specific algorithms. Carotenoids interference in stationary phase also explains the limited

BGD
11, 6119–6149, 2014

apparent linearity of chlorophyll detection by ICAM absorption to a maximum of approximately 50 $\mu g L^{-1}$ (Peperzak et al., 2011). At a high nitrogen-limited *Phaeocystis* biomass, the use of total absorption including the Carotenoids, leads to an overestimation of the chlorophyll concentration.

4.3 Fluorescence quantum efficiency

The optically measured fluorescence signal correlated well with the ex situ measured Chl *a* concentrations and, as expected, showed a relative fluorescence increase in stationary phase. Using chlorophyll estimates from the FLH and the ARP-4λ algorithms, φ in mesocosm 2 increased steadily during stationary phase by more than 100 %, from $\approx$ 0.8 to $\approx$ 1.7 % (Fig. 5). Satellite estimates of φ have a corresponding range, 0–3 % (Huot et al., 2005; Behrenfeld et al., 2009). Any correlation with μ (cell growth rate) or μ_{POC} (carbon growth rate) was lost (Fig. 6c) due to the effect of changing Carotenoids: Chl ratio as a result of nitrogen limitation. This suggests that in order to relate growth conditions and fluorescence signal strength, new optical proxies should be developed for the photon absorption and emission by individual pigments (Fawley, 1989).

Even though φ can be estimated using appropriate fluorescence and absorbance algorithms, its value will – just as Fv/Fm – not be a reliable indicator of actual nitrogen-controlled *Phaeocystis* growth rate. φ is also a diagnostic for the duration of nitrogen depletion in *Phaeocystis*, which adds to the discussion on the physiological significance of Fv/Fm and C : Chl. As the present investigation was deemed to be exemplary of the phytoplankton dynamics during the wax and wane of a short-term bloom, i.e. a fast reduction from a high concentration of the limiting nutrient towards depletion, a real-world estimate of φ might behave similar as φ_{ph} in mesocosm 2. However, in oceanic waters the supply of the limiting nutrient may be low but relatively more constant, such as by aeolian deposition of iron or by continuous heterotrophic remineralization of organic material in the water column. Given that under steady-state nitrogen-limited growth, the value of Fv/Fm in *T. pseudonana* is as high as the value in nutrient-replete cul-

BGD
11, 6119–6149, 2014

tures (Parkhill et al., 2001), the significance of φ as a physiological proxy in diatom dominated waters under such nitrogen-controlled conditions seems questionable.

On the other hand, for iron-limited phytoplankton growth, φ derived from satellite data was elevated (Behrenfeld et al., 2009), so in 82 % of the oceanic regions with a low iron deposition rate, φ appears to be a reliable remote sensing physiology proxy. This applicability of φ corresponds with that of Fv/Fm as a good physiological proxy in iron-limitation studies (Timmermans et al., 2001, 2008). Maybe Fe-limitation has a more pronounced effect on φ than limitation of the major nutrients (N, P).

It appears that insight in the euphotic ecosystem is an important factor for applicability of φ as proxy for phytoplankton productivity. For example, by knowing the approximate sequence of events during stratification and the subsequent development of a spring bloom in a biophysical model approach (Mahadevan et al., 2012), assumptions could be made on the actual (exponential) growth phase of the phytoplankton, enabling the use of φ for regional primary production estimates.

Similarly, using estimates for the nutricline depth, hence nutrient supply (Cermeno et al., 2008) in combination with optical measurements, the predictive power of φ may be improved. In addition to the bloom scenario presented in this study, steady-state nutrient-limited growth and pulsed nutrient regimes and their effects on absorbance and fluorescence should shed more light on the physiological significance of real-world estimates of φ.

The present *Phaeocystis* study is an example of how experimental studies can contribute to better global carbon production estimates. More experimental data is needed from phytoplankton species that differ in their pigment composition and in the nutrients limiting their growth (N, P, Fe). Until these issues have been resolved adequately, and new combinations with for example biophysical models have been made, we should be aware of the obscured view of phytoplankton physiology, hence marine primary production estimates using remote sensing.

BGD
11, 6119–6149, 2014

Appendix A

Absorption and fluorescence algorithms

Optical proxies were derived from water leaving radiance ($W\,m^{-2}\,nm^{-1}\,sr^{-1}$) spectra that were measured every 15 min with a TriOS RAMSES-ACC-VIS hyperspectral sensor (320–950 nm in 190 channels) at an angle 50 off nadir at 0.08 m above the water surface. Surface irradiance ($W\,m^{-2}\,nm^{-1}$), used to convert radiance ($W\,m^{-2}\,nm^{-1}\,sr^{-1}$) to reflectance ($R$, sr^{-1}), was measured prior to and after the experiment and proved to remain stable. Four reflectance spectra from the middle of the light period (13:00–14:00 h) were averaged and algorithms were applied for the estimation of absorption by chlorophyll *a* and *c* ($a_{Chl\ a}$ and $a_{Chl\ c}$) and emission near the 682 nm fluorescence band (F).

First, the Chlorophyll *c* concentration was calculated from reflectance (R) by a 4-wavelength (at λ = 450, 466, 480 and 700 nm) absorption algorithm (ARP-4$\lambda_{Chl\ c}$) that was developed and positively applied by (Astoreca et al., 2009) to detect *Phaeocystis* in the North Sea:

$$a_{Chl\ c} = a_{w,700} \times R_{700} \times \left(1/R_{466} - (1/R_{450})^{(1-w)} \times (1/R_{480})^{w}\right)\ (m^{-1}) \quad \text{(A1a)}$$

With the absorption by pure water:

$$a_{w,700} = 0.572\,m^{-1} \quad (15\,°C)\ \text{(Buiteveld et al., 1994)} \quad \text{(A1b)}$$

and the weight (w) is determined by the position of the Chl *c* absorption maximum (466 nm) relative to the two reference (baseline) wavelengths (450 and 480 nm):

$$w = (\lambda_{466,Chl\ c} - \lambda_{450})/(\lambda_{480} - \lambda_{450}) = 0.53 \quad \text{(A1c)}$$

Second, a comparable absorption algorithm (ARP-4$\lambda_{Chl\ a}$) for Chlorophyll *a* was derived after choosing the appropriate wavelengths, including the Chl *a* absorption maxi-

BGD
11, 6119–6149, 2014

mum (438 nm):

$$a_{\text{Chl }a} = a_{\text{w},700} \times R_{700} \times \left(1/R_{438} - (1/R_{425})^{(1-w)} \times (1/R_{450})^{w}\right) \ (\text{m}^{-1}) \quad \text{(A1d)}$$

With water absorption given by Eq. (A1b) and the weight (w) by:

$$w = (\lambda_{438,\text{Chl }a} - \lambda_{425})/(\lambda_{450} - \lambda_{425}) = 0.52 \quad \text{(A1e)}$$

Third, F was calculated using the Fluorescence Line Height (FLH) algorithm (Abbott and Letelier, 1999) with wavelengths from a Gaussian emission model peaking at 682 nm (Peperzak et al., 2011) as:

$$F = R_{\text{Fmax}} - R_{\text{base}} (\text{sr}^{-1}) \quad \text{(A2a)}$$

with

$$R_{\text{base}} = R_{\text{b1}} + (\lambda_{\text{Fmax}} - \lambda_{\text{b1}}) \times ((R_{\text{b1}} - R_{\text{b2}})/(\lambda_{\text{b1}} - \lambda_{\text{b2}})) \ (\text{sr}^{-1}) \quad \text{(A2b)}$$

F_{max} is at the fluorescence peak (λ = 682 nm) in the mesocosm reflectance spectra (example data are shown in Peperzak et al., 2011). R_{base} is the baseline reflectance value at F_{max}, calculated linearly from the reflectance between R_{b1} and R_{b2} with b_1 = 650 nm and b_2 = 710 nm.

Phytoplankton quantum efficiency φ_{ph} is defined as the ratio of mol photons emitted as fluorescence divided by the mol photons absorbed by the pigments and is, therefore, dimensionless (Huot et al., 2005). First the Fluorescence Line Height was multiplied by the irradiance spectrum to obtain a baseline corrected radiance above water at 682 nm. Subsequently the signal was corrected for the water-air transition, absorption by water, self-absorption by the phytoplankton and converted to photons. Finally, the signal was integrated over 4π (assuming isotropic emission) and over the spectral range (650–710 nm), assuming a Gaussian distribution with a FWHM of 25 nm. See (Peperzak et al., 2011) for a more extensive validation of this conversion. At the bottom

BGD
11, 6119–6149, 2014

of each mesocosm a TriOS RAMSES-ACC-VIS hyper-spectral sensor was mounted that registered the irradiance every 15 min. From this signal the wavelength-dependent attenuation in the mesocosm was derived, that could be well reconstructed based on the ICAM absorption measurements (Figs. 6 and 8 in Peperzak et al., 2011), and the total number of absorbed photons was calculated.

Acknowledgements. We gratefully acknowledge the help of the following NIOZ personnel. S. Oosterhuis performed HPLC photo-pigment analyses. POC and PON were analyzed by S. Crawford. Nutrients were analyzed by K. Bakker, E. van Weerlee and J. van Ooijen. B. Hoogland (Van Hall Larenstein college, Leeuwarden, the Netherlands) assisted in sampling and sample analysis. We acknowledge the useful comments of Anita Buma (U. Groningen, the Netherlands) on an earlier version of the ms. H. J. v. d. W. was supported by the BSIK Climate Changes Spatial Planning A6 project. Financial support for this research was obtained from NWO project EO-078: "Improved quantification of Southern Ocean diatoms as indicators for Carbon fixation", granted to H. J. v. d. W.

References

Abbott, M. R. and Letelier, R. M.: Algorithm theoretical basis document chlorophyll fluorescence (MODIS product number 20), NASA, 1999.

Astoreca, R., Rousseau, V., Ruddick, K., Knechciak, C., van Mol, B., Parent, J.-Y., and Lancelot, C.: Development and application of an algorithm for detecting *Phaeocystis globosa* blooms in the Case 2 Southern North Sea waters, J. Plankton Res., 31, 287–300, 2009.

Behrenfeld, M. J., Boss, E., Siegel, D. A., and Shea, D. M.: Carbon-based ocean productivity and phytoplankton physiology from space, Global Biochem. Cy., 19, GB1006, doi:10.1029/2004GB002299, 2005.

Behrenfeld, M. J., Westberry, T. K., Boss, E. S., O'Malley, R. T., Siegel, D. A., Wiggert, J. D., Franz, B. A., McClain, C. R., Feldman, G. C., Doney, S. C., Moore, J. K., Dall'Olmo, G., Milligan, A. J., Lima, I., and Mahowald, N.: Satellite-detected fluorescence reveals global physiology of ocean phytoplankton, Biogeosciences, 6, 779–794, doi:10.5194/bg-6-779-2009, 2009.

BGD
11, 6119–6149, 2014

Buiteveld, H., Hakvoort, J. M. H., and Donze, M.: The optical properties of pure water, P. Soc. Photo-Opt. Ins., 2258, 174–183, 1994.
Buma, A. G. J., Bano, N., Veldhuis, M. J. W., and Kraay, G. W.: Comparison of the pigmentation of two strains of the prymnesiophyte *Phaeocystis* sp., Neth, J. Sea Res., 27, 173–182, 1991.
Carder, K. L., Chen, R., and Hawes, S.: Algorithm theoretical basis document: instantaneous photosynthetically available radiation and absorbed radiation by phytoplankton, Version 7, NASA, 24, 2003.
Cermeno, P., Dutkiewicz, S., Harris, R. P., Follows, M., Schofield, O., and Falkowski, P. G.: The role of nutricline depth in regulating the ocean carbon cycle, P. Natl. Acad. Sci. USA, 105, 20344–20349, doi:10.1073/pnas.0811302106, 2008.
Cloern, J. E., Grenz, C., and Vidergar-Lucas, L.: An empirical model of the phytoplankton chlorophyll : carbon ratio-the conversion factor between productivity and growth rate, Limnol. Oceanogr., 40, 1313–1321, 1995.
DiTullio, G. R., Grebmeier, J. M., Arrigo, K. R., Lizotte, M. P., Robinson, D. H., Leventer, A., Barry, J. P., VanWoert, M. L., and Dunbar, R. B.: Rapid and early export of *Phaeocystis antarctica* blooms in the Ross Sea, Antarctica, Nature, 404, 595–598, 2000.
Edwards, V. R., Tett, P., and Jones, K. J.: Changes in the yield of chlorophyll *a* from dissolved available inorganic nitrogen after an enrichment event – applications for predicting eutrophication in coastal waters, Cont. Shelf. Res., 23, 1771–1785, 2003.
Falkowski, P. G., Dubinsky, Z., and Wyman, K.: Growth-irradiance relationships in phytoplankton, Limnol. Oceanogr., 30, 311–321, 1985.
Falkowski, P., Greene, R. M., and Geider, R.: Physiological limitations on phytoplankton productivity in the ocean, Oceanogr. Mar. Biol., 5, 84–91, 1992.
Fawley, M. W.: A new form of chlorophyll *c* involved in light-harvesting, Plant. Physiol., 91, 727–732, 1989.
Field, C. B., Behrenfeld, M. J., Randerson, J. T., and Falkowski, P.: Primary production of the biosphere: integrating terrestrial and oceanic components, Science, 281, 237–240, 1998.
Fujiki, T. and Taguchi, S.: Variability in chlorophyll *a* specific absorption coefficient in marine phytoplankton as a function of cell size and irradiance, J. Plankton Res., 24, 859–874, 2002.
Heath, M. R., Richardson, K., and Kiørboe, T.: Optical assessment of phytoplankton nutrient depletion, J. Plankton Res., 12, 381–396, 1990.

BGD
11, 6119–6149, 2014

Huot, Y., Brown, C. A., and Cullen, J. J.: New algorithms for MODIS sun-induced chlorophyll fluorescence and a comparison with present data products, Limnol. Oceanogr.-Meth., 3, 108–130, 2005.
Kiefer, D. A.: Chlorophyll *a* fluorescence in marine centric diatoms: responses of chloroplasts to light and nutrient stress, Mar. Biol., 23, 39–46, 1973.
Kromkamp, J. and Foster, R. M.: The use of variable fluorescence measurements in aquatic ecosystems: differences between multiple and single turnover measuring protocols and suggested terminology, Eur. J. Phycol., 38, 103–112, 2003.
Kruskopf, M. and Flynn, K. J.: Chlorophyll content and fluorescence responses cannot be used to gauge reliably phytoplankton biomass, nutrient status or growth rate, New Phytol., 169, 525–536, 2006.
Lubac, B., Loisel, H., Guiselin, N., Astoreca, R., Artigas, L. F., and Meriaux, X.: Hyperspectral and multispectral ocean color inversions to detect *Phaeocystis globosa* blooms in coastal waters, J. Geophys. Res., 113, C06026, doi:10.1029/2007JC004451, 2008.
Mahadevan, A., D'Asaro, E., Lee, C., and Perry, M. J.: Stratification Initiates North Atlantic Spring Phytoplankton Blooms, Science, 337, 54–58, 2012.
Martinez-Vicente, V., Dall'Olmo, G., Tarran, G., Boss, E., and Sathyendranath, S.: Optical backscattering is correlated with phytoplankton carbon across the Atlantic Ocean, Geophys. Res. Lett., 40, 1154–1158, doi:10.1002/grl.50252, 2013.
Parkhill, J.-P., Maillet, G., and Cullen, J. J.: Fluorescence-based maximal quantum yield for PSII as a diagnostic of nutrient stress, J. Phycol., 37, 517–529, 2001.
Peperzak, L.: Daily irradiance governs growth rate and colony formation of *Phaeocystis* (Prymnesiophyceae), J. Plankton Res., 15, 809–821, 1993.
Peperzak, L.: The Wax and Wane of *Phaeocystis globosa* Blooms, Rijksuniversiteit Groningen, Groningen, the Netherlands, 254 pp., 2002.
Peperzak, L., Duin, R. N. M., Colijn, F., and Gieskes, W. W. C.: Growth and mortality of flagellates and non-flagellate cells of *Phaeocystis globosa* (Prymnesiophyceae), J. Plankton Res., 22, 107–120, doi:10.1093/plankt/22.1.107, 2000a.
Peperzak, L., Gieskes, W. W. C., Duin, R. N. M., and Colijn, F.: The vitamin B requirement of *Phaeocystis globosa* (Prymnesiophyceae), J. Plankton Res., 22, 1529–1537, 2000b.
Peperzak, L., Timmermans, K. R., Wernand, M. R., Oosterhuis, S., and Van der Woerd, H. J.: A mesocosm tool to optically study phytoplankton dynamics, Limnol. Oceanogr.-Meth., 9, 232–244, 2011.

BGD
11, 6119–6149, 2014

Rousseau, V., Mathot, S., and Lancelot, C.: Calculating carbon biomass of *Phaeocystis* sp. from microscopic observations, Mar. Biol., 107, 305–314, 1990.
Sathyendranath, S., Stuart, V., Nair, A., Oka, K., Nakane, T., Bouman, H., Forget, M.-H., Maass, H., and Platt, T.: Carbon-to-chlorophyll ratio and growth rate of phytoplankton in the sea, Mar. Ecol.-Prog. Ser., 383, 73–84, 2009.
Seoane, S., Zapata, M., and Orive, E.: Growth rates and pigment patterns of haptophytes isolated from estuarine waters, J. Sea Res., 62, 286–294, 2009.
Smith, W. O., Codispoti, L. A., Nelson, D. M., Manley, T., Buskey, E. J., Niebauer, H. J., and Cota, G. F.: Importance of *Phaeocystis* blooms in the high-latitude ocean carbon cycle, Nature, 352, 514–516, 1991.
Staehr, P. A., Henriksen, P., and Markager, S.: Photoacclimation of four marine phytoplankton species to irradiance and nutrient availability, Mar. Ecol.-Prog. Ser., 238, 47–59, 2002.
Timmermans, K. R., Davey, M. S., van der Wagt, B., Snoek, J., Geider, R. J., Veldhuis, M. J. W., Gerringa, L. J. A., and De Baar, H. J. W.: Co-limitation by iron and light of *Chaeotoceros brevis, C. dichaeta* and *C. calcitrans* (Bacillariophyceae), Mar. Ecol.-Prog. Ser., 217, 287–297, 2001.
Timmermans, K. R., Veldhuis, M. J. W., Laan, P., and Brussaard, C. P. D.: Probing natural iron fertilization near the Kerguelen (Southern Ocean) using natural phytoplankton assemblages and diatom cultures, Deep-Sea-Res. I I., 55, 693–705, 2008.
Vogt, M., O'Brien, C., Peloquin, J., Schoemann, V., Breton, E., Estrada, M., Gibson, J., Karentz, D., Van Leeuwe, M. A., Stefels, J., Widdicombe, C., and Peperzak, L.: Global marine plankton functional type biomass distributions: *Phaeocystis* spp., Earth Syst. Sci. Data, 4, 107–120, doi:10.5194/essd-4-107-2012, 2012.
Wassmann, P., Vernet, M., Mitchell, B. G., and Rey, F.: Mass sedimentation of *Phaeocystis pouchetii* in the Barents Sea, Mar. Ecol.-Prog. Ser., 66, 183–195, 1990.

BGD
11, 6119–6149, 2014

Table 1. List of used variables, measurements and computations.

Symbol	Description	Measurement or Computation	Units
a_{ph}	Phytoplankton (total pigment) absorption coefficient	Integrating cavity absorption meter, from 400 to 672 nm	m^{-1}
$a_{Chl\ a\ (c)}$	Chlorophyll *a* or *c* absorption coefficient	ARP $(-4\lambda)(-\text{Chl}\ a/c)$ 4-wavelength algorithm from reflectance spectrum (Eq. A1)	m^{-1}
a_{Chl}	Total chlorophyll absorption coefficient	$a_{Chl\ a} + a_{Chl\ c}$	m^{-1}
$a^*_{Chl\ a\ (c)}$	Chlorophyll *a* or c-specific absorption coefficient	a_{ph}/Chl *a* (at 428 or 674 nm) or a_{ph}/Chl *c* (at 466 nm) (Table 2)	$m^{-2}\,(mg\,Chl)^{-1}$
C : Chl (*a*)	Carbon to Chlorophyll (*a*) ratio	POC/Chl or POC/Chl *a*	$g\,g^{-1}$
C : N	Carbon to Nitrogen ratio	POC/PON	mol mol^{-1}
Carotenoids	Sum of fucoxanthin, diatoxanthin, diadinoxanthin, β, ε- and β, β-carotene	HPLC	$\mu g\,L^{-1}$
C : cell	Carbon content per cell	POC/N_t	pg $cell^{-1}$
Carots: Chl	Carotenoids to chlorophyll ratio	Carots/Chl	Unitless
Chl *a*	Chlorophyll-a	HPLC	$\mu g\,L^{-1}$
Chl *c*	Chlorophyll-c	HPLC	$\mu g\,L^{-1}$
Chl	Sum of Chl *a* and Chl *c*	HPLC	$\mu g\,L^{-1}$
Chl *a*(*c*) : cell	Chl *a* (*c*) content per cell	Chl *a* (*c*)/N_t	pg $cell^{-1}$
DIN	Dissolved Inorganic Nitrogen	Continuous flow chemistry	$\mu mol\,L^{-1}$
F	Chlorophyll *a* fluorescence	Fluorescence Line Height algorithm (Eq. A2)	sr^{-1}
F_0	Dark-adapted chlorophyll fluorescence	Pulse Amplitude Modulation fluorometer	Unitless
F_v/F_m	Photosystem II quantum efficiency	Pulse Amplitude Modulation fluorometer	Unitless
$N_{t,(t+1)}$	Cell concentration on day t $(t+1)$	Flow cytometer	cells μL^{-1}
N : cell	Nitrogen content per cell	PON/N_t	pg $cell^{-1}$
POC	Particulate Organic Carbon	Mass spectrometer	$\mu g\,L^{-1}$
PON	Particulate Organic Nitrogen	Mass spectrometer	$\mu g\,L^{-1}$
R	Reflectance	Water-leaving radiance/Surface irradiance	sr^{-1}
SRP	Soluble Reactive Phosphate	Continuous flow chemistry	$\mu mol\,L^{-1}$
φ_{ph}	Quantum efficiency of fluorescence using phytoplankton absorption	$(F\ a_{ph}) \times 100\,\%$	%
μ	Cell specific growth rate between day_t and day_{t+1}	$\ln(N_{t+1}/N_t)/(day_{t+1} - day_t)$	day^{-1}
μ_{POC}	Carbon specific growth rate between day_t and day_{t+1}	$\ln(POC_{t+1}/POC_t)/(day_{t+1} - day_t)$	day^{-1}

BGD
11, 6119–6149, 2014

Table 2. *Phaeocystis* chlorophyll-specific absorption coefficients peaks in $m^2\,(mg\,Chl)^{-1}$ during exponential and stationary growth. Listed are averages ±95 % confidence intervals.

Mesocosm number	*N*	Day	Growth phase	$a^*_{Chl\ a}$ (438 nm)	$a^*_{Chl\ c}$ (466 nm)	$a^*_{Chl\ a}$ (674 nm)
1 + 2	6	2–4	Exponential	0.053 ± 0.005	0.044 ± 0.005	0.026 ± 0.003
1	4	10–13	Stationary	0.081 ± 0.012	0.059 ± 0.003	0.033 ± 0.004
2	4	10–13	Stationary	0.091 ± 0.015	0.058 ± 0.004	0.036 ± 0.005

BGD
11, 6119–6149, 2014

Table 3. Linear regression equations of *Phaeocystis* absorption on HPLC-measured chlorophyll *a* and *c* concentrations. Absorption was calculated with the ARP-4λ-Chl *a* and ARP-4λ-Chlc algorithms (Eq. A1). Regressions were made for the mesocosms separately, for exponential (day 0–4) and stationary (day 5–14) growth phases. Indicated are slope and intercepts ±95 % confidence interval.

		N	Slope ($\times 10^{-3}$)	Intercept ($\times 10^{-3}$)	R^2
Chl *a*	Mesocosm 1	15	1.2 ± 0.1	-0.6 ± 2.8	0.94
Chl *a*	Mesocosm 2	15	1.4 ± 0.2	-3.1 ± 3.5	0.91
Chl *a*	Exponential	10	1.4 ± 0.1	-1.3 ± 1.8	0.98
Chl *a*	Stationary	20	1.4 ± 0.3	-4.4 ± 5.0	0.82
Chl *a*	Stationary[a]	19	1.4 ± 0.3	-4.6 ± 5.4	0.80
Chl *a*	Combined	30	1.3 ± 0.1	-1.8 ± 2.0	0.92
Chl *c*	Mesocosm 1	15	1.5 ± 0.2	2.0 ± 6.2	0.88
Chl *c*	Mesocosm 2	15	1.7 ± 0.4	-1.0 ± 8.6	0.80
Chl *c*	Exponential	10	1.8 ± 0.2	1.3 ± 2.9	0.98
Chl *c*	Stationary	20	1.8 ± 0.6	-6.7 ± 14.7	0.59
Chl *c*	Stationary*	19	1.6 ± 0.6	-4.0 ± 14.6	0.56
Chl *c*	Combined	30	1.6 ± 0.2	0.6 ± 4.9	0.84

* Day 9 of mesocosm 1 excluded (1 day after nutrient-spike).

BGD
11, 6119–6149, 2014

Table 4. Linear regression equations of *Phaeocystis* fluorescence on HPLC- measured chlorophyll *a* concentrations. Fluorescence was calculated with the FLH-H algorithm (Eq. A2). Regressions were made for the mesocosms separately, for exponential (day 0–4) and stationary (day 5–14) growth phases. Indicated are slopes and intercepts ±95 % confidence intervals.

		N	Slope ($\times 10^{-2}$)	R^2
Chl *a*	Mesocosm 1	15	2.6 ± 0.4	0.93
Chl *a*	Mesocosm 2	15	3.4 ± 0.8	0.88
Chl *a*	Exponential	10	3.1 ± 0.8	0.88
Chl *a*	Stationary	20	1.4 ± 1.1	0.27
Chl *a*	Combined	30	2.9 ± 0.5	0.81

BGD
11, 6119–6149, 2014

Table 5. Biochemical characteristics of *Phaeocystis* in the mesocosm compared to published data from cultures, unless otherwise indicated. Chl is the sum of chlorophyll *a* and *c*; Fuco = fucoxanthin.

Variable	Unit	Mesocosm	Published/Field	reference
Carbon content	pg cell^{-1}	10–40	11	Rousseau et al. (1990)
Chlorophyll *a*	pg cell^{-1}	0.1–0.2	0.1–0.3[a]	Buma et al. (1991)
			1.8[a]	
Chlorophyll *c*	pg cell^{-1}	0.1–0.2	0.3[a]	Buma et al. (1991)
			0.8[a]	Astoreca et al. (2009)
C : Chl *a*	g:g	60–500	16–400[b]	Falkowski et al. (1985)
			65–111[c]	Sathyendranath et al. (2009)
C : Chl	g:g	30–200	–	–
Chl *c* : Chl *a*	g:g	1.1–1.9	0.1–0.8[e]	Buma et al. (1991)
			0.4	Astoreca et al. (2009)
			0.4	Seoane et al. (2009)
Fuco : Chl *a*	g:g	1.2–2.2	0.2–0.3[d]	Astoreca et al. (2009)
			0.3–0.8[e]	Buma et al. (1991)
			0.3–1.0[d]	Seoane et al. (2009)

[a] For larger non-flagellated *Phaeocystis* cells.
[b] Range of 3 species cultured at different irradiances.
[c] C : Chl *a* for prymnesiophytes in field samples determined by regression analysis.
[d] High value at low irradiance.
[e] In Marsdiep during *Phaeocystis* blooms (Wadden Sea tidal inlet).

BGD
11, 6119–6149, 2014

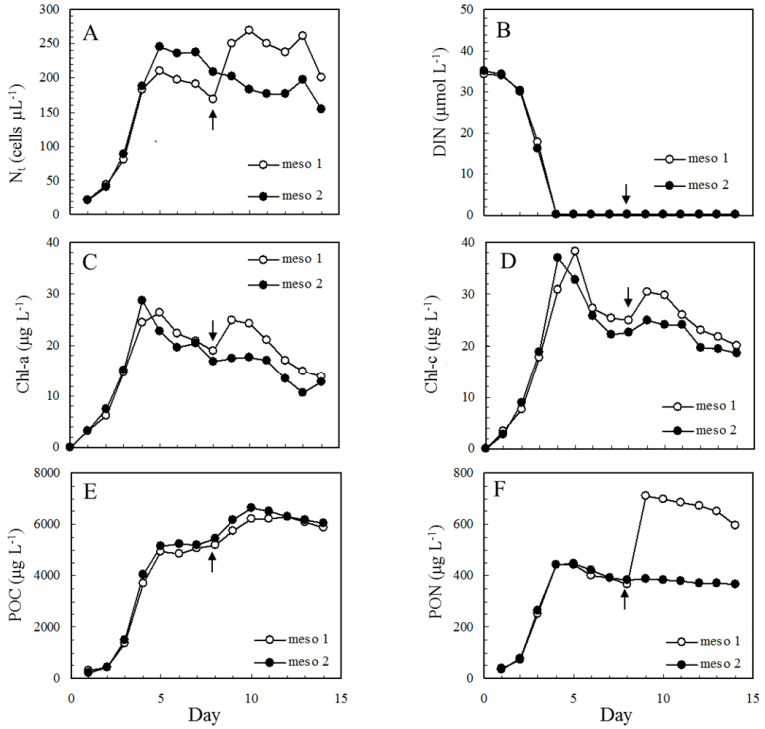

Fig. 1. (A–F) *Phaeocystis*, nutrient and carbon dynamics in two mesocosms (meso 1, meso 2) in time. **(A)** Cell abundances (cells µL^{-1}), **(B)** Dissolved Inorganic Nitrogen (DIN, µmol L^{-1}), **(C)** Chlorophyll *a* (Chl *a*, µg L^{-1}), **(D)** Chlorophyll *c* (Chl *c*, µg L^{-1}), **(E)** Particulate Organic Carbon (POC, µg L^{-1}), **(F)** Particulate Organic Nitrogen (PON, µg L^{-1}). The arrow indicates the nutrient addition to mesocosm 1 after sampling on day 8.

BGD
11, 6119–6149, 2014

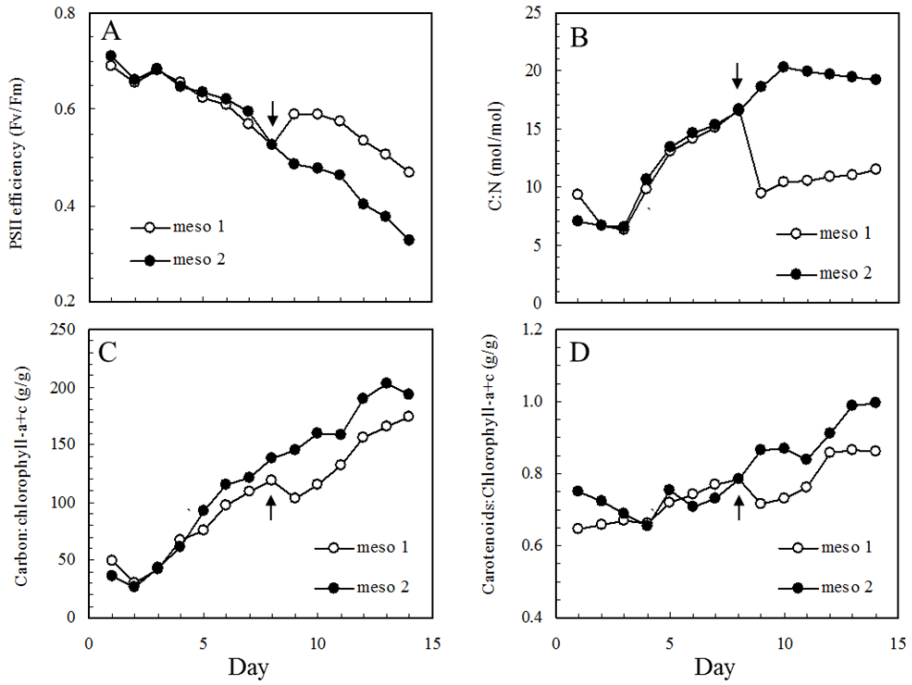

Fig. 2. (A–D) *Phaeocystis* physiology and pigment ratios in two mesocosms in time. **(A)** Photosystem II efficiency (Fv/Fm), **(B)** Carbon to Nitrogen ratio (C : N, mol mol^{-1}), **(C)** Carbon to Chlorophyll *a* +*c* ratio (C : Chl *a* + *c*, g g^{-1}), **(D)** Carotenoids to Chlorophyll *a* + *c* ratio (g g^{-1}). The arrow indicates the nutrient addition to mesocosm 1 after sampling on day 8.

BGD
11, 6119–6149, 2014

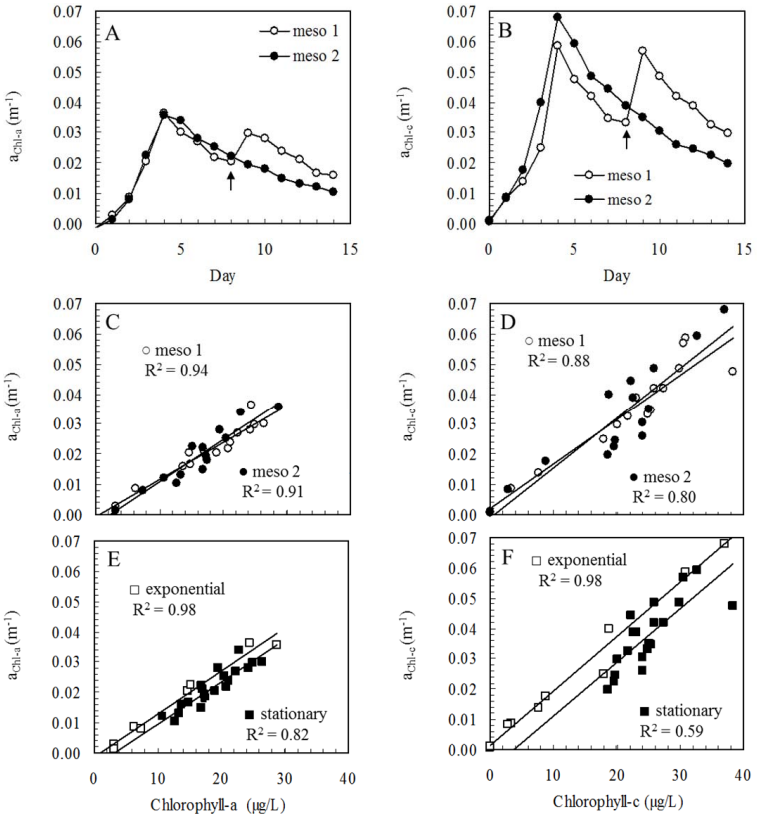

Fig. 3. (A–F) Absorption characteristics in *Phaeocystis*. **(A–B)**: temporal development (days) of absorption by chlorophyll *a* (**A** $a_{\mathrm{Chl}\ a}$, m^{-1}) and *c* (**B** aChl *c*, m^{-1}) calculated from reflectance spectra in both mesocosms. **(C–F)**: linear regression of absorption on chlorophyll *a* and *c* (m^{-1}) against Chl *a* and Chl *c* concentrations ($\mu\mathrm{g\,L}^{-1}$) was performed separately for both mesocosms **(C, D)** and for exponential and stationary growth phases **(E, F)**.

BGD
11, 6119–6149, 2014

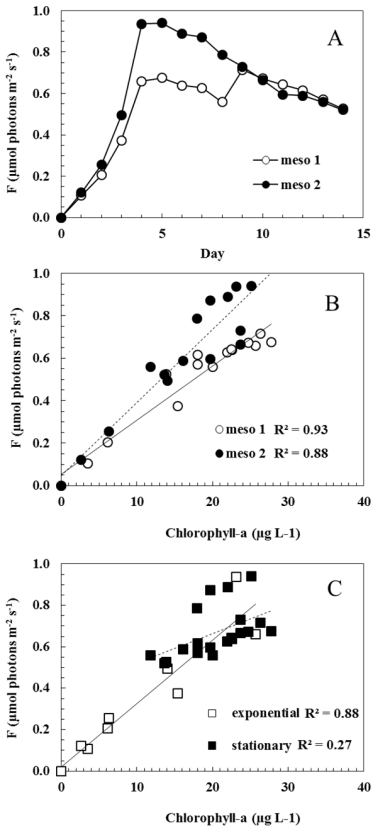

Fig. 4. (A–C) Fluorescence emission. **(A)** daily development of the fluorescence emission near 682 nm (F, µmol photons $m^{-2} s^{-1}$) calculated from reflectance spectra, **(B)** linear regression of fluorescence (F, µmol photons $m^{-2} s^{-1}$) on chlorophyll *a* (µg L^{-1}) for both mesocosms separately and **(C)** for both exponential and stationary growth phases.

BGD
11, 6119–6149, 2014

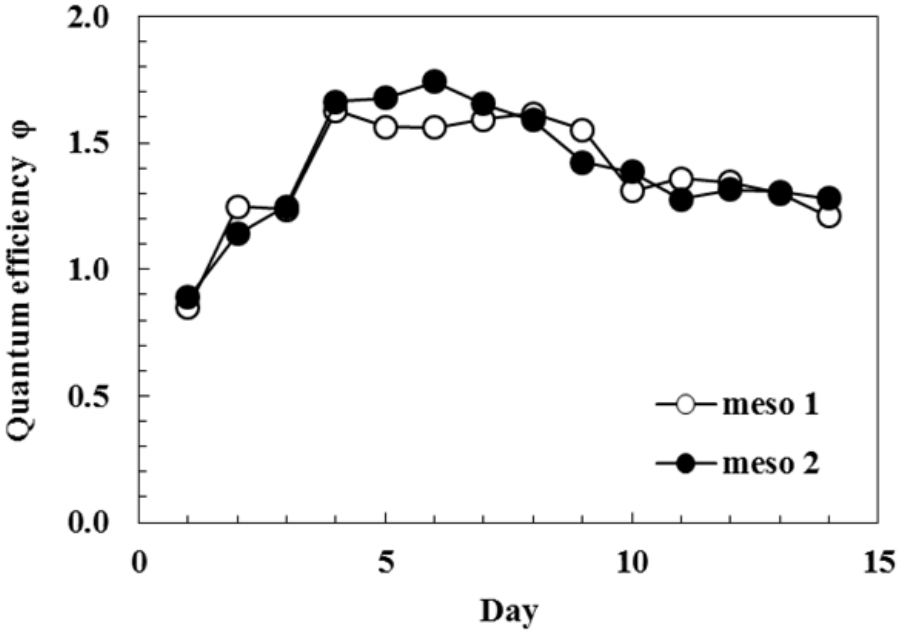

Fig. 5. Development in time (days) of quantum efficiency φ_{ph} derived from total phytoplankton absorption and fluorescence in two mesocosms.

BGD
11, 6119–6149, 2014

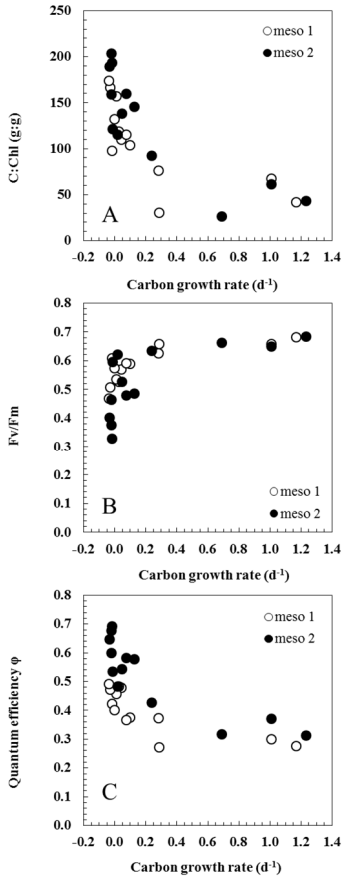

Fig. 6. Three proxies for growth rate as function of measured carbon growth rate (μ_{POC}, d^{-1}): **(A)**: carbon to Chlorophyll *a*+*c* ratio (**C**: Chl *a*+*c*, $g g^{-1}$), **(B)**: Photosystem II efficiency (Fv/Fm) and **(C)**: quantum efficiency (φ, %). Data combined from both mesocosms.

BGD
11, 6119–6149, 2014